Journal of Power Sources 247 (2014) 170–177

Contents lists available at ScienceDirect

Journal of Power Sources

journal homepage: www.elsevier.com/locate/jpowsour

Improved microstructure and performance of Ni-based anode for intermediate temperature solid oxide fuel cells

Bin Hua, Wenying Zhang, Meng Li, Xin Wang, Bo Chi, Jian Pu, Jian Li*

Center for Fuel Cell Innovation, School of Materials Science and Engineering, State Key Laboratory of Material Processing and Die & Mould Technology, Huazhong University of Science and Technology, Wuhan, Hubei 430074, China

HIGHLIGHTS

- Ni-based anodes were prepared by NiO impregnation, (Ni, Mg)O impregnation and conventional sintering.
- They are investigated under the conditions of anodic current polarization and redox cycling.
- Optimized loading of impregnation was obtained as 40 wt%.
- Improved performance stability and redox-ability were achieved by (Ni, Mg)O impregnation.

ARTICLE INFO

Article history:
Received 2 May 2013
Received in revised form
14 August 2013
Accepted 17 August 2013
Available online 3 September 2013

Keywords:
Solid oxide fuel cell
Ni based anode
Impregnation
Performance durability
Redox-ability

ABSTRACT

Three kinds of anodes prepared by NiO impregnation, (Ni, Mg)O impregnation and conventional sintering methods are investigated under the conditions of anodic current polarization and redox cycling. The optimized NiO loading in the NiO-impregnated anode is 40 wt%; and the minimum polarization resistance is 1.40, 0.71 and 0.60 Ω cm^2 at 700, 750 and 800 °C, respectively, due to the increased triple phase boundary and conductivity that promote the charge-transfer process of H_2 oxidation reaction. The conventional Ni–YSZ cermet anode is less sensitive to the current polarization at 200 mA cm^{-2}; however, its polarization resistance is much higher than those of the impregnated anodes. (Ni, Mg)O impregnation improves the performance durability and redox-ability at 800 °C, with a low polarization resistance of 0.93 Ω cm^2 after 48 h of current polarization and of 0.71 Ω cm^2 after 10 redox cycles. The addition of Mg lowers the reducibility of (Ni, Mg)O particles; and its improved electrochemical performance and redox cycling resistance are attributed to its stabilized microstructure consisting of nano-scale Ni particles distributed on the surface of the pre-sintered YSZ scaffold. The agglomeration of fine Ni particles is suppressed by the unreduced (Ni, Mg)O in the anode.

1. Introduction

Solid oxide fuel cells (SOFCs) are a highly efficient energy conversion device which generates electrical power directly from fossil, biomass and hydrocarbon fuels at a low level of greenhouse gas emission. Fuel flexibility is one of their major advantages over other types of fuel cells. In a SOFC cell, the fuel is oxidized at the porous anode and subsequently reacts with the oxygen ions (O^{2-}) incoming from the electrolyte, which requires the anode materials to be electrocatalytically active and ionically and electronically conductive. Among the state-of-the-art anode materials, Ni–Y_2O_3 stabilized ZrO_2 (Ni–YSZ) cermet is the most widely and frequently used due to its high catalytic activity and electrical conductivity [1–4]. In this cermet anode, Ni provides the desired catalytic activity and electronic conductivity, while YSZ offers the oxygen ion conductivity and adjusts the coefficient of thermal expansion (CTE). Ni–YSZ anodes possess excellent electrochemical performance in H_2 fuel, compared to other types of anode materials; however, they are suffering from carbon deposition and sulfur poisoning in hydrocarbon fuels, and destructive structure evolution caused by the redox and Ni particle agglomeration. To enhance the resistance of Ni–YSZ anodes to carbon deposition and sulfur poisoning, tremendous efforts have made by element alloying [5–13] and oxide addition [14–16]. In comparison, much less attention has been paid to increase their resistance to the structural degradation.

* Corresponding author. Tel.: +86 27 87557694; fax: +86 27 87558142.
E-mail addresses: plumarrow@126.com, lijian@hust.edu.cn (J. Li).

0378-7753/$ – see front matter © 2013 Elsevier B.V. All rights reserved.
http://dx.doi.org/10.1016/j.jpowsour.2013.08.060

Operated at relatively high temperatures, Ni in the anode is oxidized to NiO when it is exposed to an oxidizing atmosphere by accident or due to high fuel utilization overbalancing the equilibrium between Ni and NiO; and the NiO will be subsequently reduced to Ni when the normal anode atmosphere is resumed. Such a redox cycle is accompanied by a volume change of more than 60%, which generates stresses in functional anode and anode support, even in the layer of electrolyte. Repeated redox cycling will result in dimensional instability and more seriously cracking and structural disintegration of the cell [17–19]. In addition, high temperature operation causes microstructural changes of Ni–YSZ anodes featured by the growth of Ni particles [20–23]. The anode reaction in Ni–YSZ anode can only occur on the contact lines between Ni and YSZ, that is, the triple phase boundaries (TPB) where electrons, oxide ions and gaseous fuel meet each other. The coarsening of Ni particles due to continuous sintering along with the operation will reduce the length of the TPB and the electronic conductivity of the anode [20]; consequently the electrocatalytic activity of the anode is decreased and in turn the cell performance is compromised.

To enhance the resistance of Ni–YSZ anodes to the redox, an alternate method, solution impregnation, was adopted to fabricate the anode in the present study. The wet method has been proved effective in preparing high performance nano-structured anodes [24] and cathodes [25–28], compared with the conventional sintering method [29,30]. With Ni particles infiltrated on a sintered YSZ scaffold, the anode dimension is fixed by the scaffold, which remains invariant during redox cycles and maintains the structural integrity of the anode [31]. However, the impregnated Ni particles are still susceptible to isothermal instability caused by Ni particle agglomeration, leading to anode structure and performance degradation. This suggests the necessity of stabilizing the Ni particles in the impregnated Ni + YSZ anode to ensure its long-term performance.

In conventional Ni–YSZ cermet anode, MgO was considered as an additive to stabilize Ni particles against sintering and promote hydrocarbon reforming [32–36]. The results indicate that the reforming of hydrocarbon and biogas was enhanced [32,33,35] and the microstructure of the anode was stabilized [35,36] by the addition of MgO. As to the electrochemical performance, Shiratori et al. [33] observed a degradation by adding MgO due to increase in ohmic resistance of the anode material; however, Phongaksorn et al. [34] reported an increased peak power density for a cell with MgO-added Ni cermet anode because of a much lower polarization resistance of the anode, even though the ohmic resistance of the anode was increased. As a matter of fact, the ohmic resistance is not an issue in the impregnated anode as long as the loading of Ni is above the threshold for 3-D percolation. In the present study, MgO was co-impregnated with NiO to form (Ni, Mg)O + YSZ anode, with the purpose of stabilizing the microstructure and enhancing the electrochemical performance of the Ni-based cermet anode. In this paper, the optimization of impregnation loading, the redox-ability, microstructure evolution and electrochemical performance of the impregnated anodes were reported, in comparison with that of the conventional Ni cermet anode.

2. Experimental

2.1. Cell preparation

Electrolyte supported button cells were prepared as a vehicle for anode evaluations. The electrolyte substrate was fabricated by dry pressing 8%mol YSZ powder (TZ8YS, Tosoh) in a cylindrical die, followed by sintering at 1500 °C in air for 5 h. The sintered dense YSZ substrate was approximately 22 mm in diameter and 1.3 mm in thickness. For preparation of a nano-structured Ni + YSZ anode via solution impregnation, a porous YSZ layer was firstly fabricated on the sintered YSZ substrate by the screen printing-sintering process. The screen-printed YSZ slurry contained 15 wt% of carbon black as the pore former and was sintered at 1250 °C in air for 1 h. The porous YSZ layer was 10–20 μm thick with an area of 0.5 cm^2, to which Ni^{2+} or Ni^{2+} and Mg^{2+} containing solution was infiltrated. The solution was made by dissolving pure $Ni(NO_3)_2{\cdot}6H_2O$ or $Ni(NO_3)_2{\cdot}6H_2O$ and $Mg(NO_3)_2{\cdot}6H_2O$ at a molar ratio of 0.9 to 0.1 into distilled water to reach a concentration of 0.3 M. Being dried in air and calcined at 600 °C in air for 1 h, the impregnated solution was converted to nano-sized NiO or $Ni_{0.9}Mg_{0.1}O$ oxide particles. The weight ratio of impregnated oxide to YSZ in the anode was between 20 and 50 wt% controlled by the injected volume of the solution via a syringe. For the purpose of comparison, the conventional Ni–YSZ cermet anode was also prepared by screen-printing a slurry containing NiO and YSZ at a weight ratio of 50 to 50 on the sintered electrolyte substrate and sintering at 1350 °C in air for 2 h. For convenience, all the cells prepared for the present study were classified by fabrication method and composition, as listed in Table 1, in which the volume percentage of Ni (vol% (Ni)) in the reduced anode was estimated by the following equation

$$\mathrm{Vol\%(Ni)} = \frac{\mathrm{vol(Ni)}}{\mathrm{vol(Ni)+vol(YSZ)}} = \frac{\frac{M(\mathrm{Ni})}{D(\mathrm{Ni})}}{\frac{M(\mathrm{Ni})}{D(\mathrm{Ni})}+\frac{M(\mathrm{YSZ})}{D(\mathrm{YSZ})}} \times 100\% \quad (1)$$

where the *V*, *M* and *D* represent the volume, weight and density of each component, respectively.

2.2. Electrochemical measurement

To evaluate the electrochemical performance of the prepared anode, Pt paste was symmetrically painted on the electrolyte substrate opposite to the anode (working electrode) and baked at 750 °C in air for 1 h, as the counter and reference electrodes. The distance between the round counter electrode and the ring-like reference electrode was 4 mm, which was approximately 3 times the thickness of the electrolyte substrate, satisfying the extreme measurement requirement in the three-electrode configuration [37]. Pt mesh and wire were used as the current collector and measuring lead; and a Ceramabond glass sealant (Aremco Product, Inc.) was used to seal the anode compartment. The electrochemical performance of the reduced anode was characterized by using an impedance/gain phase analyzer (Solartron 1260) and an electrochemical interface (Solartron 1287) at temperatures between 700 and 800 °C and a constant hydrogen flow of 100 ml min^{-1}. The AC amplitude was 10 mV, and the frequency was in the range between 10^{-2} and 10^6 Hz. To understand the effect of electrical current on the anode performance, anodic current polarization at 200 mA cm^{-2} was also conducted at 750 °C; and the impedance data were acquired at an interval of 3 h.

Table 1
Prepared Cells with various kinds of anodes and compositions.

Cell no.	Anode	Composition (wt%)	Ni (wt%)	Ni (vol%)
1	Conventional	NiO/YSZ = 50/50	44	34
2	Impregnated	NiO/YSZ = 20/80	16	12
3		NiO/YSZ = 30/70	25	18
4		NiO/YSZ = 40/60	34	26
5		NiO/YSZ = 50/50	44	34
6	Impregnated	(Ni, Mg)O/YSZ = 40/60 (wt%) Ni/Mg = 90/10 (at%)		

2.3. Redox test

To compare the redox-ability of the conventional and impregnated anodes, the prepared anodes were subjected to redox cycles. After initial impedance measurement in pure H_2 at 800 °C and subsequent N_2 flushing for 15 min, the anode was oxidized in air for 30 min by flowing air into the anode compartment, which was then flushed by N_2 for another 15 min before the anode was reduced in flowing pure H_2 for 30 min. The flow rate of all the gases used in the test was fixed at 100 ml min^{-1} and electrochemical impedance measurement was performed at an interval of 5 redox cycles.

2.4. Microstructure and phase characterization

The microstructure of the anodes was examined by using a scanning electron microscope (SEM, Sirion 200); and the phases in the anodes were identified by X-ray diffraction (XRD, X'Pert Pro, PAN Analytical B.V.) at room temperature with a Cu Kα radiation. The range of the 2θ angle was between 20 and 70°, and the scan rate was 10° min^{-1}.

3. Results and discussions

3.1. Optimization of catalyst loading in impregnated anode

The electrochemical performance of the anodes was characterized by electrochemical impedance spectrum (EIS). Fig. 1 shows the open circuit EIS (Nyquist plot) of impregnated anodes with various NiO loadings (Cell-2 to Cell-5) in dry H_2 at temperatures of 700, 750 and 800 °C. The spectra were featured by flatten arcs, which intercepted with the real axis at high and low frequencies,

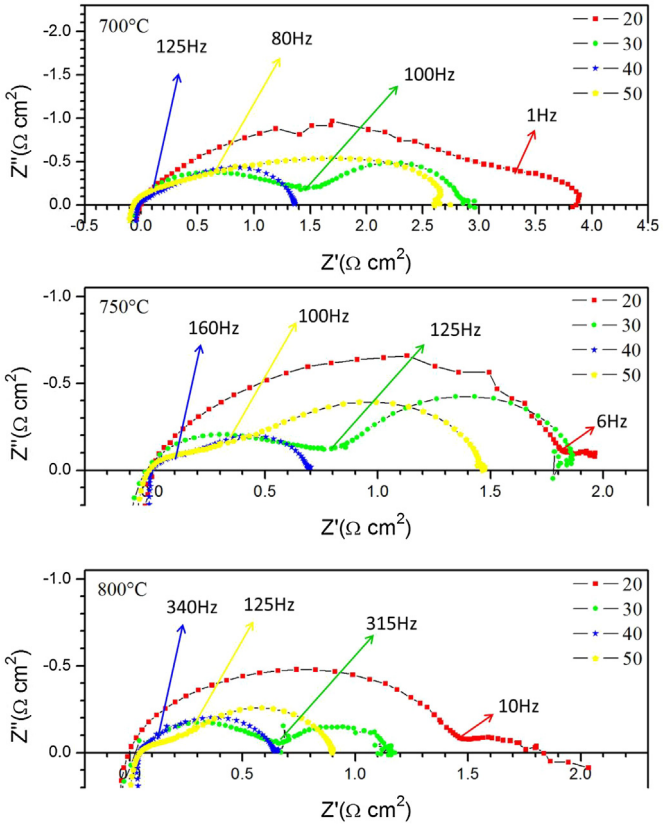

Fig. 1. Electrochemical impedance spectra measured in H_2 at open circuit and temperatures of 700, 750 and 800 °C for NiO-impregnated anodes with different NiO contents (wt%).

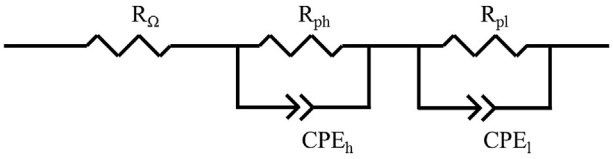

Fig. 2. Equivalent circuit used for fitting the impedance spectra shown in figure.

representing the ohmic (R_Ω, mainly contributed by electrolyte) and total (R_T) resistances of the cell, respectively. The difference between R_T and R_Ω is the polarization resistance (R_P), measuring the electrochemical performance of the anode. It is seen that increasing temperature decreased the value of R_P, due to the enhanced anode activity by temperature. For example, the R_P value of the anode containing 20 wt% loaded NiO decreased from 3.91 to 1.79 Ω cm^2 as temperature increased from 700 to 800 °C. It is also noticed from Fig. 1 that increasing the loading of NiO reduced the value of R_P until a minimum was achieved at 40 wt% loaded NiO. It was 1.40, 0.71 and 0.60 Ω cm^2 at 700, 750 and 800 °C, respectively, exhibiting a comparable electrochemical performance to the conventional Ni–Gd_2O_3 doped CeO_2 (Ni–GDC) anode [16,38]. However, further increasing the amount of loaded NiO to 50 wt% increased the value of R_P. This result indicates that there exists a limiting level of loaded NiO for the impregnated Ni + YSZ anode, at which the electrochemical performance of the anode is maximized.

For getting more insight into the effect of loaded NiO on the performance of the impregnated anode, the electrochemical impedance spectra shown in Fig. 1 were deconvoluted into two arcs by using an equivalent circuit shown in Fig. 2, similarly to what reported in Ref. [16,34]. R_{Ph} and CPE_h are the electrode resistance and constant phase element associated with the high-frequency arc, and R_{Pl} and CPE_l are those associated with the low-frequency arc. As known, H_2 oxidation reaction on a Ni–YSZ anode is mainly comprised of two consecutive processes, that is, H_2 diffusion and dissociation, followed by charge transfer over the Ni/YSZ interface [16,39]. The first step is strongly influenced by the catalyst, while the second one is dependent on the mixed (electronic and ionic) conductivity of the anode at the triple phase boundary [40]. It is generally accepted that the high-frequency arc is related to the charge transfer process at the Ni/electrolyte interface; and the low-frequency impedance arc is related to H_2 diffusion and dissociation in the electrode [39,40].

The values of R_{Ph} and R_{Pl} determined by data fitting for various anodes at different temperatures were listed in Table 2; and the characteristic frequency separating the high- and low-frequency

Table 2
Polarization resistance of impregnated anodes at various temperatures.

Anode	Temperature (°C)	R_P (Ω cm^2)	R_{Ph} (Ω cm^2)	R_{Pl} (Ω cm^2)
NiO/YSZ = 20/80	700	3.9119	3.3370	0.5749
	750	2.1823	1.8570	0.3253
	800	1.7950	1.5100	0.2850
NiO/YSZ = 30/70	700	2.8700	1.4570	1.4130
	750	1.8451	0.8646	0.9805
	800	1.0995	0.5066	0.5929
NiO/YSZ = 40/60	700	1.4027	0.2108	1.1919
	750	0.7048	0.1031	0.6017
	800	0.6003	0.0672	0.5331
NiO/YSZ = 50/50	700	2.6999	0.9954	1.7045
	750	1.4700	0.4132	1.0568
	800	0.8599	0.2259	0.6340
Ni–MgO/YSZ	700	1.3800	1.0999	0.2801
	750	0.8100	0.3499	0.4601
	800	0.6200	0.1989	0.4211

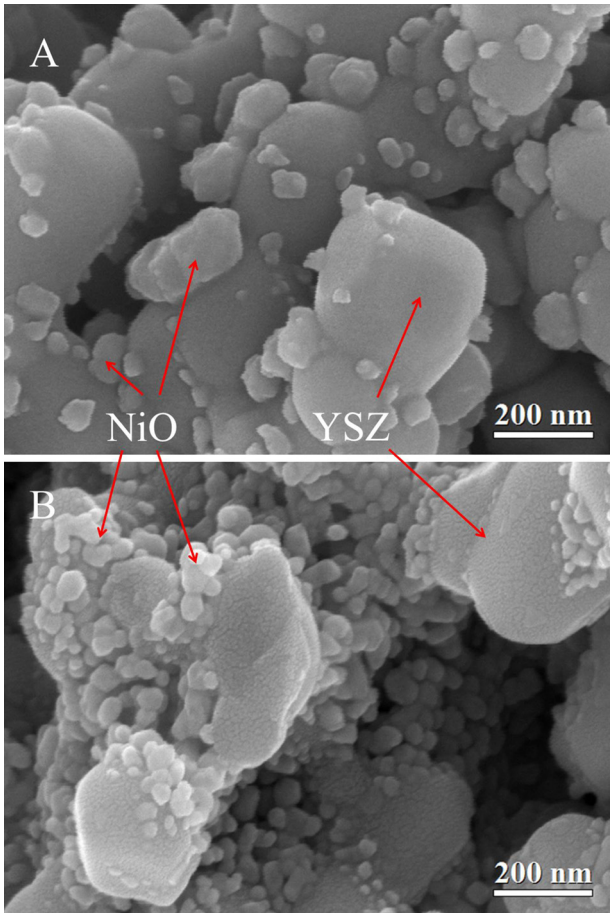

Fig. 3. SEM micrographs showing microstructures of 20 wt% NiO-impregnated (A) and 40 wt% NiO-impregnated (B) before reduction.

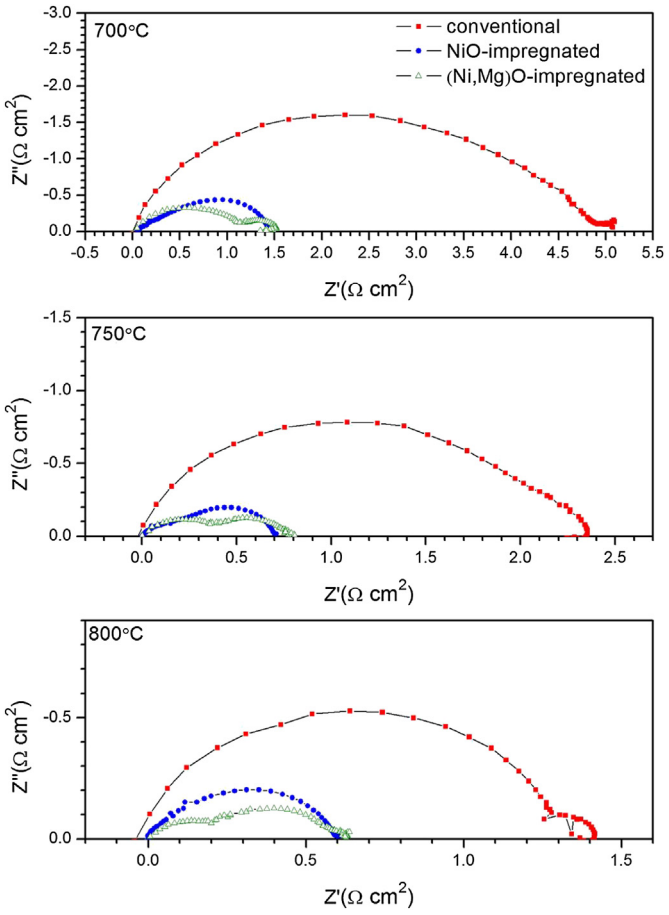

Fig. 4. Electrochemical impedance spectra measured in H_2 at open circuit and temperatures of 700, 750 and 800 °C for various kinds of anodes: Conventional, NiO-impregnated and (Ni, Mg)O-impregnated. The loading in impregnated anodes is 40 wt%.

arcs was marked in Fig. 1. The results indicate that the high-frequency polarization resistance reduced and the low-frequency one fluctuated as NiO loading was increased up to 40 wt%; and further increasing the loaded NiO to 50 wt% increased both the polarization resistances. This phenomenon can be explained by the evolution of anode microstructure with the increase of NiO loading. At a low level of NiO loading, such as 20 wt% (Fig. 3a), NiO particles were sporadically distributed on the surface of YSZ scaffold and the TPB for H_2 oxidation was inadequate, leading to a higher R_{Ph}; and at a higher level of NiO loading, for example 40 wt% (Fig. 3b), the TPB was significantly increased, resulting in a much lower R_{Ph}. The fluctuation of R_{Pl} was probably due to the competing effect between H_2 diffusion and dissociation. The former prefers a low level of NiO loading and high anode porosity, and the latter prefers a high level of NiO loading with a larger Ni surface area. Increasing NiO loading to the level of 50 wt%, the surface of YSZ scaffold was excessively covered by Ni, significantly reducing the TPB, exposed Ni surface and the porosity of the anode; consequently both high- and low-frequency polarization resistances were increased. Based on the EIS results shown in Fig. 1, the anode with 40 wt% loaded NiO was selected for further evaluation, together with the conventional and (Ni, Mg)O-impregnated anodes.

3.2. Durability of electrochemical performance

Fig. 4 compares the initial EIS of the conventional Ni–YSZ cermet anode (Cell 1), 40 wt% NiO impregnated anode (Cell 4) and 40 wt% $Ni_{0.9}Mg_{0.1}O$ impregnated anode (Cell 6). To focus on the electrochemical performance of the anode, the R_Ω was subtracted. The overall polarization resistance (R_P) of Cell 1 was 4.18, 2.34 and 1.56 Ω cm^2 at 700, 750 and 800 °C, respectively, which fall into the R_P range of Ni–YSZ anodes [1,16], but are significantly higher than those of the impregnated anodes. This result can be understood

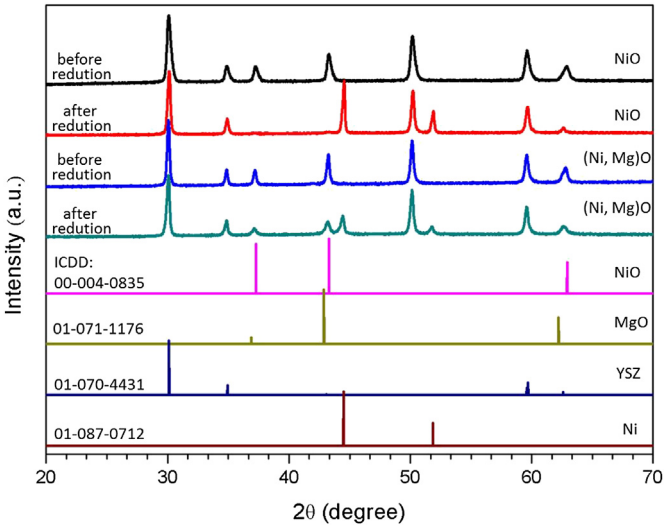

Fig. 5. X-ray diffraction patterns of impregnated anodes before and after reduction in H_2 at 750 for 2 h. The loading in impregnated anodes is 40 wt%.

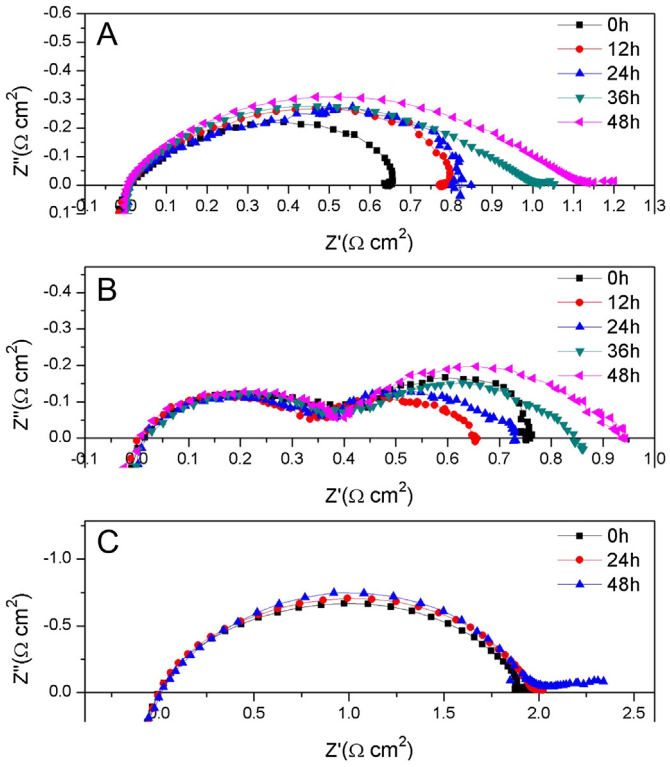

Fig. 6. Electrochemical impedance spectra of NiO-impregnated (A) and (Ni, Mg)O-impregnated (B) and conventional (C) anodes polarized at 750 °C under an anodic current of 200 mA cm^{-2} for up to 48 h. The loading in impregnated anodes is 40 wt%.

from the microstructure point of view that the TPB and the exposed Ni surface were significantly enhanced in the impregnated anodes. The (Ni, Mg)O impregnated anode demonstrated similar polarization resistance (1.38, 0.81 and 0.62 Ω cm^2 at 700, 750 and 800 °C, respectively) to that of the NiO impregnated one. Fig. 5 shows the X-ray diffraction patterns of the impregnated anodes before and after reduction at 750 °C in pure hydrogen for 2 h. It is not surprising that both the impregnated anodes contained YSZ and NiO (or (Ni, Mg)O) before reduction, and dissolution of 10 mol% MgO in NiO caused slightly left-shift of (Ni, Mg)O diffraction peaks compared with those of pure NiO. Being exposed to H_2 at 750 °C for 2 h, the pure NiO particles were fully reduced to metallic Ni; however, the (Ni, Mg)O particles were only partially reduced with some remained as (Ni, Mg)O. This result is in agreement with what reported by Tikekar et al. [41] and Shiratori et al. [35] that the reducibility of NiO was dramatically lowered by Mg addition. The existence of oxide in the reduced anode made the high- and low-frequency processes more distinguishable without significantly change the overall electrochemical performance of the anode.

To evaluate the performance durability of the impregnated anodes, they were subjected to anodic current polarization at 200 mA cm^{-2} and 750 °C for up to 48 h, with the conventional Ni–YSZ cermet anode as a comparison. Similar results were obtained in repeated tests, as typically shown in Fig. 6. It is obvious that the R_P of all three anodes increased as a result of polarization for 48 h; however, they behaved differently. For the NiO-impregnated anode, in which NiO was fully reduced to Ni before the polarization, the R_P was 0.64 Ω cm^2 initially and increased continuously with polarization time. It rose by 25% to 0.80 Ω cm^2 during the first 24 h of polarization and to 1.22 Ω cm^2 at the end of the 48 h test with a total 90% increase. In the (Ni, Mg)O-impregnated anode, the oxide was partially reduced to Ni with the presence of a certain amount of (Ni, Mg)O particles. The R_P was 0.73 Ω cm^2 in the beginning of the polarization test, and it reduced to 0.65 Ω cm^2 during the first 12 h test and then increased to 0.71 Ω cm^2 during the next 12 h test and finally increased to 0.93 Ω cm^2 at the end of the 48 h polarization, leading to a total increase of 27%. Comparing the behavior of these two electrodes, it can be concluded that (Ni, Mg)O-impregnated anode is significantly stabilized. The conventional Ni–YSZ anode was less sensitive to current polarization than the impregnated anodes, with an almost unchanged R_P value around 2.00 Ω cm^2 during the polarization test. However, This value is more than twice

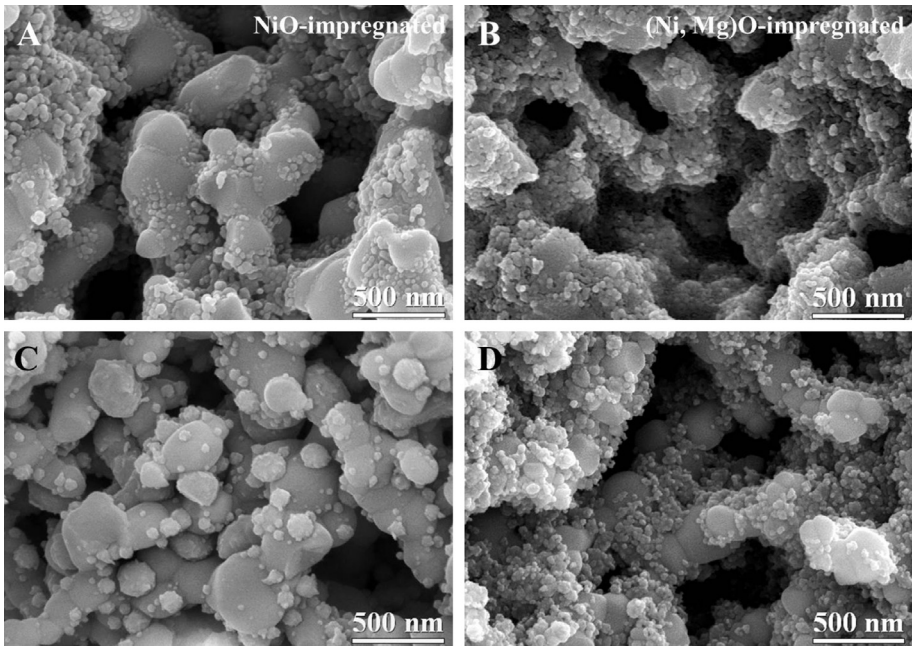

Fig. 7. SEM micrographs showing microstructures of NiO- and (Ni, Mg)O-impregnated anodes before (A, B) and after (C, D) current polarization at 200 mA cm^{-2} and 750 °C for 48 h. The loading in impregnated anodes is 40 wt%.

that of the (Ni, Mg)O-impregnated anode, suggesting that impregnating (Ni, Mg)O is an effective approach to enhance and stabilize the electrochemical performance of Ni–YSZ anode.

The electrochemical performance of the anodes is closely related to their microstructures. From microstructure point of view, it is expected that current polarization at 750 °C had a two-fold effect on anode performance. The positive effect was that the current polarization improves the contact between Ni and YSZ, which enhanced electrochemical performance of the electrode. Nevertheless it also imposed a negative effect simultaneously on the performance due to continuous sintering of the reduced Ni particles; consequently, the length of TPB and the interconnection of Ni particles, and in turn the electrode performance were decreased. The submicron-scale microstructure of the conventional Ni–YSZ cermet anode was relatively stable under the condition of the current polarization; therefore its performance remained almost unchanged. The microstructure of the impregnated anodes, consisting of nanosized Ni particles distributed on the surface of YSZ scaffold, was quite different from that of the conventional one; and their performance was eventually affected adversely by the current polarization. In the case of the NiO-impregnated anode the positive effect of current polarization on the performance was concealed by the negative effect from the beginning of the polarization; whereas for the (Ni, Mg)O-impregnated anode the positive effect was just slightly overbalanced by the negative one. Fig. 7 shows the microstructure of the impregnated anodes before and after the 48 h polarization. Prior to the polarization the reduced particles with a size below 100 nm were finely distributed on the surface of YSZ scaffold, and the reduced (Ni, Mg)O particles was somewhat smaller. Polarized for 48 h the fine particles in the NiO-impregnated anode were dramatically agglomerated to much larger particles due to Ni sintering, and those in (Ni, Mg)O-impregnated anode only grew insignificantly due to the presence of unreduced (Ni, Mg)O particles. The difference in the polarized microstructure between these two impregnated anodes explains their difference in performance stability.

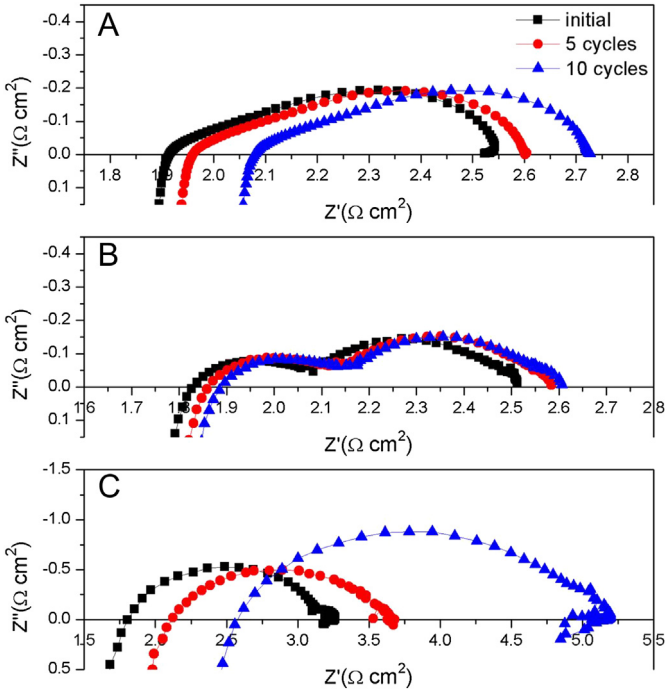

Fig. 8. Electrochemical impedance spectra of NiO-impregnated (A) and (Ni, Mg)O-impregnated (B) and conventional (C) anodes subjected to redox cycling at 800 °C. The loading in impregnated anodes is 40 wt%.

3.3. Resistance to redox cycling

Fig. 8 presents the EIS of the three kinds of anodes after redox cycling at 800 °C, showing the changes in both the R_Ω and R_P. After first 5 redox cycles, the increase in R_Ω was 0.03, 0.02 and 0.3 Ω cm^2 for the NiO-impregnated, (Ni, Mg)O-impregnated and conventional anodes, respectively; and the corresponding increase in R_P was

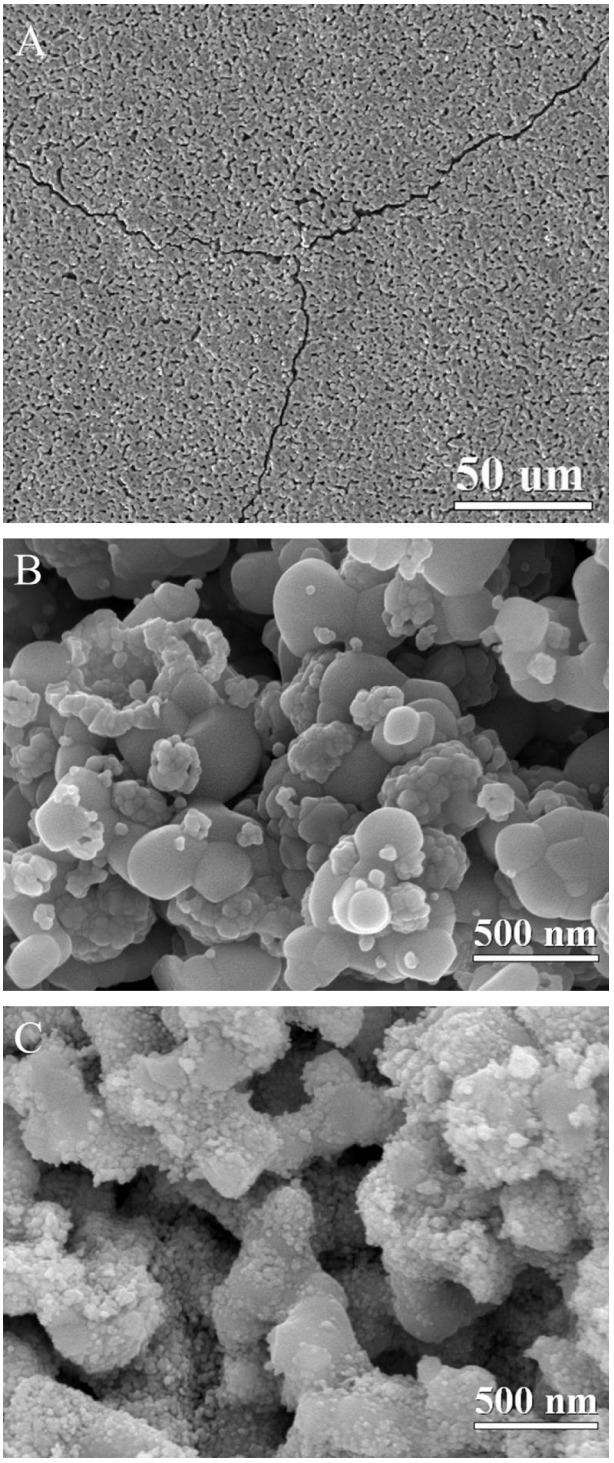

Fig. 9. SEM micrographs showing microstructures of NiO-impregnated (A) and (Ni, Mg)O-impregnated (B) and conventional (C) anodes after 10 redox cycles at 800 °C. The loading in impregnated anodes is 40 wt%.

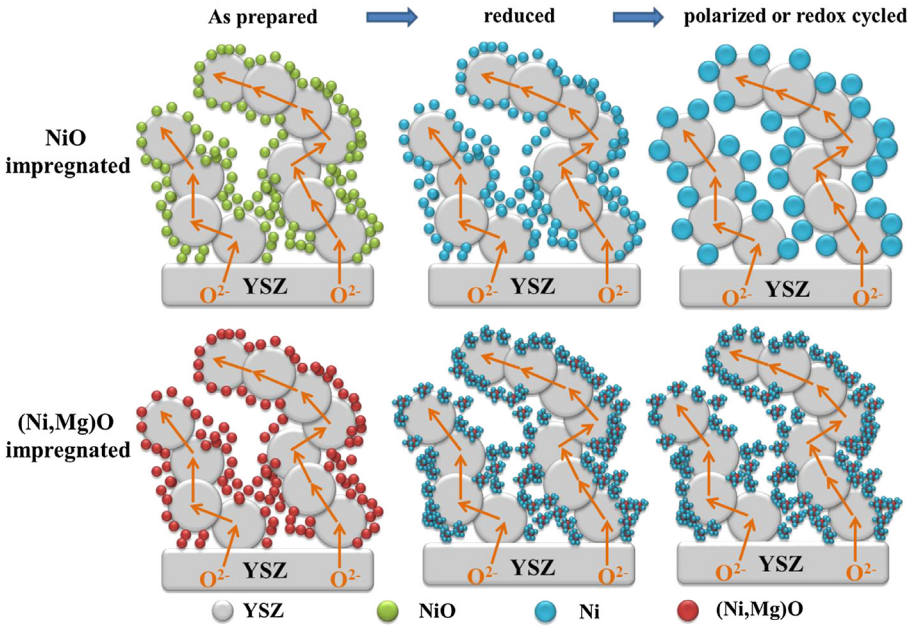

Fig. 10. Schematics showing microstructure evolution of NiO- and (Ni, Mg)O-impregnated anodes upon current polarization or redox cycling.

insignificant for the impregnated anodes, and was 1.55 Ω cm^2 for the conventional anode. After another 5 redox cycles, both NiO-impregnated and conventional anodes demonstrated a significant increase in both the R_Ω and R_P to 2.08 and 0.65, and 2.55 and 2.66 Ω cm^2, respectively. Those for the (Ni, Mg)O-impregnated anode was only moderately increased to 1.88 and 0.71 Ω cm^2. These results confirm that the impregnated anodes were more tolerant to the redox than the conventional anode; and the (Ni, Mg)O-impregnated anode possessed the highest redox-ability among these three anodes. Compared with the increase in polarization resistance of the redox-resistant $(La_{0.75}Sr_{0.25})Cr_{0.5}Mn_{0.5}O_{3-\delta}$ oxide anode (16% increase after 4 redox cycles [42]), the impregnated anodes demonstrated an excellent redox ability.

Fig. 9 shows the microstructure of the three anodes after 10 redox cycles. In the conventional anode, NiO or Ni was part of the sintered porous structure, interconnecting with the YSZ segments. The stresses arisen from the large volume change (more than 60%) accompanied with Ni ↔ NiO transformation were accumulated with the redox cycling, and eventually damaged the interfaces of Ni/YSZ in the anode and anode/electrolyte in the cell, leading to an increase in both the R_Ω and R_P and more seriously the cracking of the anode and electrolyte as shown in Fig. 9A. Unlike what in the conventional anode, the porous YSZ scaffold was sintered to the dense electrolyte in advance, and the catalyst particles were then impregnated into the pores of the scaffold via solution. The Ni ↔ NiO transformation upon redox was occurred on the surface of the YSZ scaffold, and the associated volume change would not build up a notably high level of stresses in the scaffold to detach the anode and electrolyte or disintegrate the cell. The increase in the R_Ω and R_P caused by redox cycling is attributed to the agglomeration of the reduced Ni particles, as shown in Fig. 9B. The particle agglomeration of Ni decreased the degree of 3-dimensional interconnection among the Ni particles and the length of TPB. Because of the existence of unreduced (Ni, Mg)O particles, the coalescence of reduced Ni particles was considerably suppressed, as shown in Fig. 9C, which maintained a finely interconnected distribution of Ni particles on the YSZ scaffold. As a consequence, the electrochemical performance of the (Ni, Mg)O-impregnated anode was not drastically impacted by the redox.

3.4. Microstructural stability of impregnated anodes

From above results, it is convinced that the improved electrochemical performance and redox-ability of the (Ni, Mg)O-impregnated anode over the other two anodes is ascribed to its stabilized fine Ni particles. From the viewpoint of wettability, Ni is not perfectly wettable on the surface of YSZ and turns to agglomerate thermodynamically. It was reported that the addition of oxides, such as TiO_2, Cr_2O_3 or Mn_2O_3, improved the wettability either by modification of YSZ surface [43] or by formation of unreduced Me_xO_y (Me = Ti, Cr or Mn) as an "oxide frame" [44], suppressing Ni particle growth in its metallic form due to sintering. Shiratori et al. [35] also reported that the addition of MgO into NiO formed a stable (Ni, Mg)O solution, which was incompletely reduced to fine Ni particles with retained (Ni, Mg)O. Based on the results from the previous studies and the microstructure observation shown in Figs. 7 and 9, a model of microstructure evolution along with the current polarization and redox cycling was proposed for the impregnated anodes, as shown in Fig. 10. The micron-scale YSZ scaffold was integrated to the electrolyte substrate by sintering and acts as a backbone of the electrode for conducting oxide ions; and NiO-based oxides were impregnated onto the surface of the backbone as a catalyst. The microstructure of this backbone would not change upon the current polarization and redox cycling. Without the addition of Mg, the initially reduced fine Ni particles in the NiO-impregnated anode were quickly agglomerated due to its poor wettability on YSZ surface; and in the (Ni, Mg)O-impregnated anodes, the fine Ni particles reduced from (Ni, Mg)O were stabilized due to the presence of retained (Ni, Mg)O. It is the finely stabilized microstructure that promotes the stability of electrochemical performance and redox-ability of the (Ni, Mg)O-impregnated anode.

4. Conclusions

NiO-impregnated, (Ni, Mg)O-impregnated and conventional Ni–YSZ cermet anodes were prepared and investigated in the aspects of catalyst loading optimization, electrochemical performance durability and redox-ability. From the results obtained, the following conclusions are made.

1. The electrochemical performance of the NiO-impregnated anode is enhanced by increasing NiO loading up to 40 wt% with a minimum polarization resistance mainly due to its increased TPB and conductivity that promote the charge-transfer process of H_2 oxidation. Further increasing the loading worsens the electrochemical performance of the anode.
2. The conventional Ni–YSZ cermet anode is less sensitive to the current polarization at 200 mA cm^{-2} and 750 °C; however, its polarization resistance is much higher than those of the impregnated anodes. Addition of Mg into NiO significantly stabilizes the electrochemical performance of the impregnated anode with a much lower polarization resistance than that of the conventional anode.
3. Impregnated anodes are significantly more resistant to redox cycling at 800 °C than the conventional Ni–YSZ cermet anode; and adding Mg into NiO enhances the redox-ability of the (Ni, Mg)O-impregnated anode.
4. The improved electrochemical performance and redox-ability of the (Ni, Mg)O-impregnated anode are attributed to its stabilized microstructure consisting of nano-scale Ni particles distributed on the surface of the pre-sintered YSZ scaffold. The agglomeration of fine Ni particles is suppressed by the unreduced (Ni, Mg)O in the anode.

Acknowledgments

This research was financially supported by the National Natural Science Foundation of China (U1134001) and the National “863” Project of China (2011AA050702). SEM and XRD characterizations were performed with the assistance of the Analytical and Testing Center of Huazhong University of Science and Technology.

References

[1] S. Jiang, S. Chan, J. Mater. Sci. 39 (2004) 4405–4439.
[2] A. Atkinson, S. Barnett, R.J. Gorte, J.T.S. Irvine, A.J. McEvoy, M. Mogensen, S.C. Singhal, J. Vohs, Nat. Mater. 3 (2004) 17–27.
[3] E. Tsipis, V. Kharton, J. Solid State Electrochem. 12 (2008) 1367–1391.
[4] A.J. Jacobson, Chem. Mater. 22 (2009) 660–674.
[5] H. Kim, C. Lu, W.L. Worrell, J.M. Vohs, R.J. Gorte, J. Electrochem. Soc. 149 (2002) A247–A250.
[6] M. Boder, R. Dittmeyer, J. Power Sources 155 (2006) 13–22.
[7] S. Jung, M.D. Gross, R.J. Gorte, J.M. Vohs, J. Electrochem. Soc. 153 (2006) A1539–A1543.
[8] E. Nikolla, J.W. Schwank, S. Linic, Catal. Today 136 (2008) 243–248.
[9] E.W. Park, H. Moon, M.-S. Park, S.H. Hyun, Int. J. Hydrogen Energy 34 (2009) 5537–5545.
[10] C.M. Grgicak, M.M. Pakulska, J.S. O'Brien, J.B. Giorgi, J. Power Sources 183 (2008) 26–33.
[11] I. Gavrielatos, V. Drakopoulos, S. Neophytides, J. Catal. 259 (2008) 75–84.
[12] O.A. Marina, C.A. Coyle, M.H. Engelhard, L.R. Pederson, J. Electrochem. Soc. 158 (2011) B424.
[13] L. Jia, X. Wang, B. Hua, W. Li, B. Chi, J. Pu, S. Yuan, L. Jian, Int. J. Hydrogen Energy 37 (2012) 11941–11945.
[14] O. Costa-Nunes, R.J. Gorte, J.M. Vohs, J. Power Sources 141 (2005) 241–249.
[15] S. Choi, J. Wang, Z. Cheng, M. Liu, J. Electrochem. Soc. 155 (2008) B449.
[16] L. Zhang, S.P. Jiang, H.Q. He, X. Chen, J. Ma, X.C. Song, Int. J. Hydrogen Energy 35 (2010) 12359–12368.
[17] D. Sarantaridis, A. Atkinson, Fuel Cells 7 (2007) 246–258.
[18] M. Ettler, H. Timmermann, J. Malzbender, A. Weber, N.H. Menzler, J. Power Sources 195 (2010) 5452–5467.
[19] V. Vedasri, J.L. Young, V.I. Birss, J. Power Sources 195 (2010) 5534–5542.
[20] D. Simwonis, F. Tietz, D. Stöver, Solid State Ionics 132 (2000) 241–251.
[21] R. Vaßen, D. Simwonis, D. Stöver, J. Mater. Sci. 36 (2001) 147–151.
[22] S. Jiang, J. Mater. Sci. 38 (2003) 3775–3782.
[23] P. Tanasini, M. Cannarozzo, P. Costamagna, A. Faes, J. Van Herle, A. Hessler-Wyser, C. Comninellis, Fuel Cells 9 (2009) 740–752.
[24] J.-T. Zhang, F.-L. Liang, B. Chi, J. Pu, L. Jian, J. Power Sources 200 (2012) 29–33.
[25] F. Liang, J. Chen, J. Cheng, S.P. Jiang, T. He, J. Pu, J. Li, Electrochem. Commun. 10 (2008) 42–46.
[26] J. Chen, F. Liang, L. Liu, S. Jiang, B. Chi, J. Pu, J. Li, J. Power Sources 183 (2008) 586–589.
[27] F. Liang, J. Chen, S.P. Jiang, B. Chi, J. Pu, L. Jian, Electrochem. Solid State Lett. 11 (2008) B213.
[28] J. Chen, F. Liang, B. Chi, J. Pu, S.P. Jiang, L. Jian, J. Power Sources 194 (2009) 275–280.
[29] R. Craciun, S. Park, R.J. Gorte, J.M. Vohs, C. Wang, W.L. Worrell, J. Electrochem. Soc. 146 (1999) 4019–4022.
[30] S.P. Jiang, Mater. Sci. Eng. A 418 (2006) 199–210.
[31] A.N. Busawon, D. Sarantaridis, A. Atkinson, Electrochem. Solid State Lett. 11 (2008) B186.
[32] T. Takeguchi, Y. Kani, T. Yano, R. Kikuchi, K. Eguchi, K. Tsujimoto, Y. Uchida, A. Ueno, K. Omoshiki, M. Aizawa, J. Power Sources 112 (2002) 588–595.
[33] Y. Shiratori, K. Sasaki, J. Power Sources 180 (2008) 738–741.
[34] M. Phongaksorn, A. Yan, M. Ismail, A. Ideris, E. Croiset, S. Corbin, Y. Yoo, ECS Trans. 35 (2011) 1683–1688.
[35] Y. Shiratori, Y. Teraoka, K. Sasaki, Solid State Ionics 177 (2006) 1371–1380.
[36] E. Chinarro, F.M. Figueiredo, G.C. Mather, J.R. Jurado, J.R. Frade, J. Eur. Ceram. Soc. 27 (2007) 4233–4236.
[37] J. Winkler, P.V. Hendriksen, N. Bonanos, M. Mogensen, J. Electrochem. Soc. 145 (1998) 1184–1192.
[38] A. Babaei, S.P. Jiang, J. Li, J. Electrochem. Soc. 156 (2009) B1022.
[39] S.P. Jiang, S.P.S. Badwal, Solid State Ionics 123 (1999) 209–224.
[40] S.P. Jiang, S.P.S. Badwal, J. Electrochem. Soc. 144 (1997) 3777–3784.
[41] N.M. Tikekar, T.J. Armstrong, A.V. Virkar, J. Electrochem. Soc. 153 (2006) A654.
[42] D.M. Bastidas, S. Tao, J.T.S. Irvine, J. Mater. Chem. 16 (2006) 1603–1605.
[43] A. Tsoga, A. Naoumidis, P. Nikolopoulos, Acta Mater. 44 (1996) 3679–3692.
[44] A. Tsoga, P. Nikolopoulos, A. Naoumidis, Ionics 2 (1996) 427–434.